

## Effect of Phosphate Ions on the Surface Chemistry and Microstructure of Amorphous Alumina

Fedele Abbattista, Alessandro Delmastro, Giuseppe Gozzelino, Daniele Mazza and Mario Vallino  
Dipartimento di Scienza dei Materiali e Ingegneria Chimica, Politecnico di Torino, C. so Duca Degli  
Abruzzi, 24, 10129 Torino, Italy

Guido Busca and Vincenzo Lorenzelli  
Istituto di Chimica, Facoltà di Ingegneria, Università, P.le Kennedy, 16129 Genova, Italy

High-surface-area amorphous  $\text{Al}_2\text{O}_3\text{-AlPO}_4$  samples (P/Al ratio: 0–0.17) have been prepared by reductive decomposition of aluminium nitrate in the presence of phosphoric acid. The materials obtained are amorphous up to 1100–1200 K and present "zeolitic-type" monomodal microporosity ( $r = 10\text{--}15 \text{ \AA}$ ). They are weakly acidic. The Lewis acidity changes from being weak (associated with octahedrally coordinated  $\text{Al}^{3+}$  ions) to being strong by increasing P content due to the formation of tetrahedral  $\text{Al}^{3+}$  ions induced by phosphate species. Brønsted sites are also present; these are associated with phosphate species. The catalytic activity in methanol dehydration increases with P content up to P/Al = 10/90. P inhibits both the crystallization of the  $\gamma$ -alumina phase and the  $\gamma$ - to  $\alpha$ -alumina phase transition.

Amorphous aluminas constitute poorly known materials that are potentially useful in the field of heterogeneous catalysis.<sup>1–3</sup> In a previous paper<sup>4</sup> we have characterized high-surface-area amorphous alumina prepared by an unconventional procedure. We found that the surface acidity of this material as well as its catalytic activity in methanol dehydration is lower than that of  $\gamma$ -type crystalline alumina obtained by its crystallization. We attributed this effect to the preferential octahedral coordination of  $\text{Al}^{3+}$  ions on the amorphous material, the acidity and catalytic activity of transition aluminas being assigned to tetrahedrally coordinated  $\text{Al}^{3+}$ .<sup>4</sup> This conclusion found support in the results of Nortier *et al.*<sup>5</sup> who found predominantly octahedral ions in another amorphous alumina sample by  $^{27}\text{Al}$  MAS NMR measurements.

Alumina-based amorphous materials such as silica–alumina<sup>6</sup> and alumina–boria<sup>7</sup> are acidic materials of high technological interest in catalysis. In the first case Al is thought to be tetrahedrally coordinated<sup>6</sup> while in alumina–boria both octahedral and tetrahedral Al ions have been found by NMR.<sup>7</sup> Amorphous aluminium phosphate  $\text{AlPO}_4$  and  $\text{Al}_2\text{O}_3\text{-AlPO}_4$  mixed catalysts have been the object of increasing interest in recent years because they display relevant surface acidity and catalytic activities in several acid-catalysed reactions.<sup>8–12</sup> Al is reported to be tetrahedrally coordinated on amorphous  $\text{AlPO}_4$  as on its numerous crystalline forms,<sup>13</sup> but octahedrally coordinated Al can be present in the tetrakisphosphate as well as in the  $\text{Al}_2\text{O}_3\text{-P}_2\text{O}_5$  glasses.<sup>14</sup> Alumina samples impregnated by phosphoric acid have also been characterized: the presence of phosphate species increases the surface Brønsted acidity but only slightly perturbs the Lewis sites,<sup>15</sup> and inhibits the loss of surface area and the  $\gamma$ - to  $\alpha$ -transformation upon heating.<sup>16</sup> Therefore, it was of interest for us to investigate the effect of phosphoric acid on the bulk and surface chemistry of amorphous alumina.

### Experimental

#### Materials and Instrumentation

Glycerine, tartaric acid, aluminum nitrate  $\text{Al}(\text{NO}_3)_3 \cdot 9\text{H}_2\text{O}$ , methanol and pyridine were pure products from Carlo Erba (Milano, Italy). Pyridine was further purified by multiple freeze–pump–thaw cycles before vaporization.

Differential thermal analysis (DTA) was performed with a Netzsch 404 DTA cell equipped with a computerized 434 programmer unit.

X-Ray powder diffraction (XRD) analysis was performed with computer-aided Philips PW 1710 equipment (Cu K $\alpha$  radiation, graphite monochromator).

Infrared spectra were recorded with a Nicolet MX1 Fourier transform spectrometer equipped with a conventional gas-manipulation and an evacuation ramp. The samples for pyridine adsorption study were pressed into self-supporting disks and pretreated by heating under dynamic evacuation ( $10^{-5}$  Torr for 2 h) in the IR cell.

Surface area and pore distribution were determined through the B.E.T. adsorption isotherms of  $\text{N}_2$  at 77 K obtained with a Carlo Erba Sorptomatic 1800. The pore distribution curves were obtained from the  $\text{N}_2$  adsorption isotherm evaluating the data of the desorption cycle by means of the standard model proposed by Hasley.<sup>17</sup>

The catalytic activity in the methanol dehydration was evaluated by analysing the effluent of a tubular plug reactor (i.d. 0.25 in) through a Carlo Erba Fractovap D gas chromatograph equipped with TCD detector and an HP 3900 A integrator.

#### Preparation of Catalysts

Catalysts were obtained by the procedure reported in a previous work.<sup>4</sup> Different mixtures of aluminium nitrate, diacid ammonium phosphate and glycerine (*ca.* 10 wt % with respect to aluminium nitrate) were heated at 353 K until a melt was obtained. The liquids were heated at 453 K to decompose the nitrates and the resulting solids were treated at 670 K (2 h) in dry air.

Tartaric acid, used as a reducing agent for the preparation of pure amorphous alumina, was substituted by glycerine (10 wt %) for the preparation of P-containing materials because of the inhibition observed in the reaction between tartaric acid and aluminium nitrate in the presence of phosphate ions. In this way we obtained materials with different phosphorus contents, used in the experiments with the label  $\text{AlP}_x$ ,  $x$  referring to the atomic percentage of phosphorus [oxygen excluded;  $x = 100 \text{ P}/(\text{Al} + \text{P})$ ].

#### Catalytic Activity Evaluation

The catalytic activity of the samples was tested by isothermal runs of methanol dehydration. Liquid methanol from a

metering pump was mixed in a vaporizer in known proportions with a gaseous stream of helium and the mixture was introduced into a stainless-steel tubular reactor containing a fixed bed of alumina, 0.5–1 mm in size, obtained by crushing a pressed self-consistent sheet of material. In a typical run the catalyst was conditioned overnight at 450 K under helium flow and the methanol to dimethyl ether conversion was tested in the range 450–560 K starting from the lower temperature and increasing it in steps of 10 K. At each temperature the gas leaving the reactor was sampled and analysed by an on-line gas chromatograph. In the g.c. analytical conditions adopted (Porapak Q column at 430 K) the only reaction products detected at a level higher than 0.1% of the converted methanol were dimethyl ether and water. Data were collected only when steady-state conditions of reaction were established. The gaseous flow through the reactor was set at  $100 \text{ cm}^3 \text{ min}^{-1}$  to exclude kinetic control by external film resistance.

## Results and Discussion

### Thermo-differential Analyses and X-Ray Diffraction

The DTA runs on all samples which were pre-heated at 670 K show two exothermic peaks, one more intense and sharper at lower temperatures and another, less intense at rather high temperatures. The thermograms relative to the AlP0 and AlP10 samples are compared in Fig. 1. The positions of the maxima of the two exothermic peaks, namely  $T_1$  and  $T_2$ , do vary noticeably according to the sample composition, as shown in Fig. 2. It is evident that while  $T_1$  increases almost regularly by increasing the phosphorus content in the sample,  $T_2$  rises to a plateau at 2% phosphorus (AlP2).

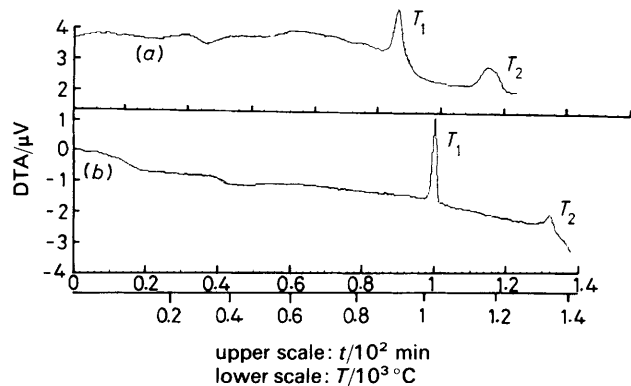


Fig. 1 Differential thermoanalysis (DTA) curves of AlP0 (a) and AlP10 (b) samples as obtained at 670 K

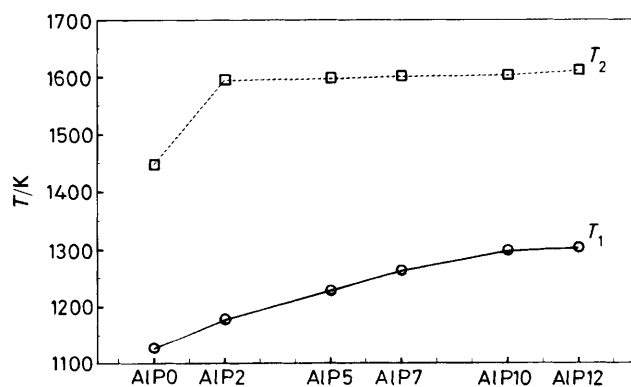


Fig. 2 Effect of the phosphorus content on the transition temperatures of amorphous samples AlP0 to AlP12 (○,  $T_1$ : amorphous to  $\gamma$ ; □,  $T_2 = \gamma$  to  $\alpha$ )

XRD analyses of samples allow us to assign these exothermic effects to two successive structural modifications of the samples. Indeed all samples when treated at temperatures 50 K lower than  $T_1$  for 1–2 h do not show any X-ray diffraction peak, as it is typical for amorphous materials [Fig. 3(a)]. All samples, when treated at temperatures between  $T_1$  and  $T_2$  display the X-ray patterns shown in Fig. 3(b) with the typical broadened peaks of  $\gamma$ -alumina (ASTM 26–93) together with at least one peak, also broadened, belonging to the  $\text{AlPO}_4$  phase in the crystalalite form (ASTM 11–500). The intensities of the  $\text{AlPO}_4$  peaks relative to those of  $\gamma$ -alumina increase with the phosphate content of the samples but are only noticeable in samples with 5 atom % phosphorus or higher. The broadness of the peaks of both phases indicates that they are badly crystallized or crystallized with extremely small crystal domains (of the order of magnitude of 10 Å). The X-ray patterns of the solids treated at temperatures 50 K higher than  $T_2$  show the well-resolved peaks of both  $\alpha$ - $\text{Al}_2\text{O}_3$  (ASTM 10–173) and of  $\text{AlPO}_4$  (crystalalite form). We can therefore conclude that the first exothermic transition at temperature  $T_1$  corresponds to a first crystallization from the amorphous mass of  $\gamma$ - $\text{Al}_2\text{O}_3$  which leaves aside badly crystallized  $\text{AlPO}_4$ . An increase in the phosphate content of the samples would hinder this transition and therefore increase the related temperature  $T_1$ ; this corresponds to the experimental evidence (see Fig. 2).

The second transformation at  $T_2$  would correspond only to structural rearrangements inside the two phases. While the  $\gamma$ - $\text{Al}_2\text{O}_3$  transforms to  $\alpha$ - $\text{Al}_2\text{O}_3$ , coarse crystallized  $\text{AlPO}_4$  rearranges also to well crystallized  $\text{AlPO}_4$  in the low crystalalite form.

This latter phenomenon is indeed not influenced by the phosphate content of the samples and occurs at nearly the same temperature (ca. 1600 K) in all the examined range, except for pure  $\text{Al}_2\text{O}_3$  (AlP0  $T_2 = 1450$  K). This could be justified by a low solubility (lower than 2 atom %) of phosphorus in the  $\gamma$ - $\text{Al}_2\text{O}_3$  phase formed from the amorphous mixture. This solubility would of course hinder the  $\gamma$ - to  $\alpha$ -

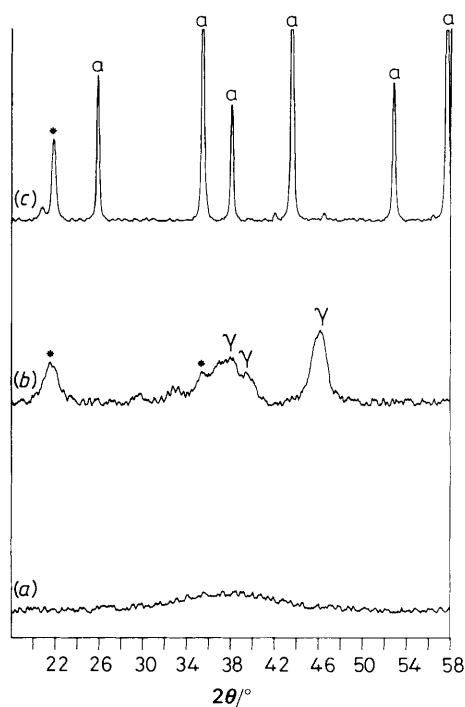


Fig. 3 X-ray patterns of AlP10 sample heat treated at different temperatures: (a) 670 K, (b) 1370 K and (c) 1570 K ( $\alpha = \alpha$ - $\text{Al}_2\text{O}_3$ ;  $\gamma = \gamma$ - $\text{Al}_2\text{O}_3$ ; \* =  $\text{AlPO}_4$ )

transformation in alumina and therefore increase the  $T_2$  temperature, to the same extent in all powders containing 2% P or more. However, a surface effect could also be hypothesized, as discussed below.

### IR Spectra (Skeletal Region)

The FTIR spectra (KBr disks) of the samples AIP0, AIP10 and AIP15 calcined at 670 K are compared in Fig. 4. In all cases a strong band is found centred in the region  $700\text{--}550\text{ cm}^{-1}$ , due to Al—O stretchings. This band is broad and structureless according to the amorphous character of the materials. P-containing powders also contain a broad absorption centred near  $1130\text{ cm}^{-1}$ , due to PO stretchings. The spectrum obtained by subtraction of that of amorphous alumina from the one of P-containing materials [Fig. 4(d)] shows that (i) the broad PO band is actually centred at  $1180\text{ cm}^{-1}$  and has a shoulder near  $1300\text{ cm}^{-1}$ ; (ii) another absorption is clearly visible at lower frequency, having a broad shoulder near  $900\text{ cm}^{-1}$  and the main broad maximum near  $815\text{ cm}^{-1}$ . This band could be tentatively assigned to the asymmetric stretching of P—O—P bridges, suggesting that phosphate groups are in part condensed.

In Fig. 5 the FTIR spectra of AIP0 (pure alumina) after calcination at 670 K (a), 1370 K (b) and 1570 K (c) are compared. The spectra (b) and (c) correspond to those reported in the literature for  $\gamma$ - and  $\alpha$ -alumina, respectively.<sup>18</sup> Thus, IR spectroscopy, which is also sensitive to amorphous materials, confirms the XRD results in relation to the phase composition of pure aluminas.<sup>4</sup> In Fig. 6 the spectra of AIP10 after heating at 1370 K (a) and 1570 K (b) are reported and compared with that of crystalline  $\text{AlPO}_4$  [crystalalite form, spectrum (c), AIP50]. These spectra can also be taken as being qualitatively representative of those of the other P-containing samples. They again confirm the XRD data, as discussed above. In fact, the poorly resolved spectrum of  $\gamma$ -alumina may be envisaged also in the spectra of AIP10 after calcination at 1370 K, while that of corundum is very evident in the sample calcined at 1570 K. However, the  $\nu\text{PO}$  band also clearly changed shape upon heating. After heating at 1370 K it is composed of a sharper band at  $1130\text{ cm}^{-1}$  (where the main  $\nu\text{PO}$  maximum of crystalline  $\text{AlPO}_4$  also falls), with a broad shoulder near  $1250\text{ cm}^{-1}$ . A relatively sharper band

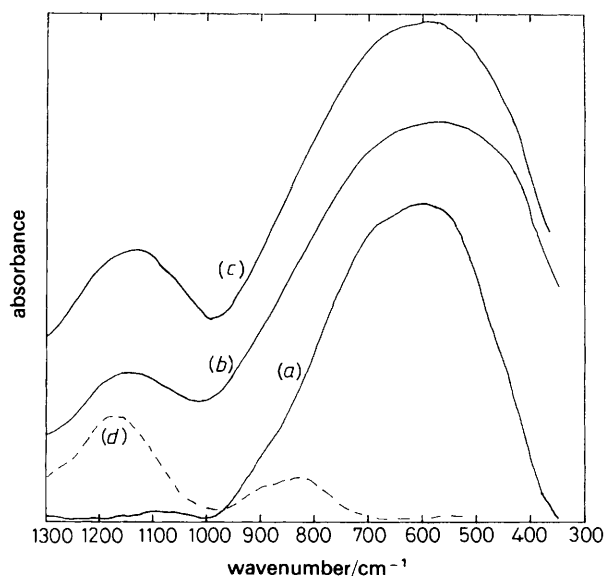


Fig. 4 FTIR spectra of AIP0 (a), AIP10 (b), AIP15 (c) and subtraction AIP10—AIP0 (d). KBr pressed disks

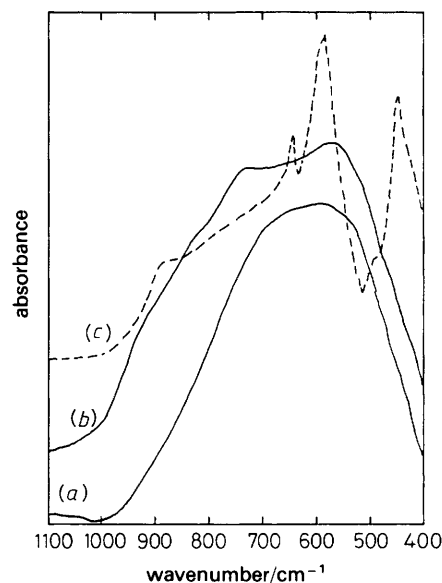


Fig. 5 FTIR spectra of AIP0 as such (a) and after calcination at 1370 K (b) and 1570 K (c). KBr pressed disks

may be observed near  $725\text{ cm}^{-1}$ ; this can be also assigned to aluminium phosphate. In crystalline  $\text{AlPO}_4$  this band is split at  $735, 715\text{ cm}^{-1}$ . It is concluded that samples treated at 1370 K are composed of  $\gamma\text{-Al}_2\text{O}_3$ , and both crystalline and amorphous  $\text{AlPO}_4$ .

Samples heated at 1570 K show [spectrum (b)] the characteristic features of both  $\alpha\text{-Al}_2\text{O}_3$  and crystalline  $\text{AlPO}_4$ , without evidence of amorphous material.

### Surface Area and Microporosity Characterization

In Table 1 the surface areas of the different amorphous samples are reported. In Fig. 7 the pore distributions of AIP0 (pure alumina), AIP2 and AIP7 after different calcination treatments are compared. At the lower temperatures (*ca.* 670 K) all samples show a monomodal distribution pattern with a sharp peak in an extremely low range,  $10\text{--}13\text{ \AA}$ . The 'zeolite-type' microporous structure of our samples compares well with that of the amorphous alumina sample described by Tournier *et al.*<sup>2</sup> Addition of phosphorus and increasing its amount does not change significantly the position of this

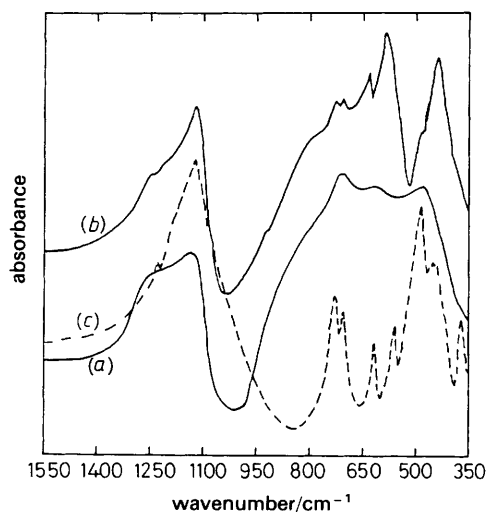


Fig. 6 FTIR spectra of AIP10 calcined at 1370 K (a) and 1570 K (b) and of  $\text{AlPO}_4$  (c)

**Table 1** Surface area ( $\text{m}^2 \text{s}^{-1}$ ) of AIP catalysts and rate for the catalytic methanol dehydration at 495 K

sample	670 K	1070 K	rate/ $10^{-3} \text{ mmol h}^{-1} \text{ m}^{-2 a}$
AIP0	364	192	7.8
AIP2	396	156	9.8
AIP5	326	—	16.8
AIP7	253	93	18.0
AIP10	191	—	33.1
AIP12	109	—	2.3
AIP15	82	—	2.2

<sup>a</sup> Catalysts treated at 670 K; (—) not determined.

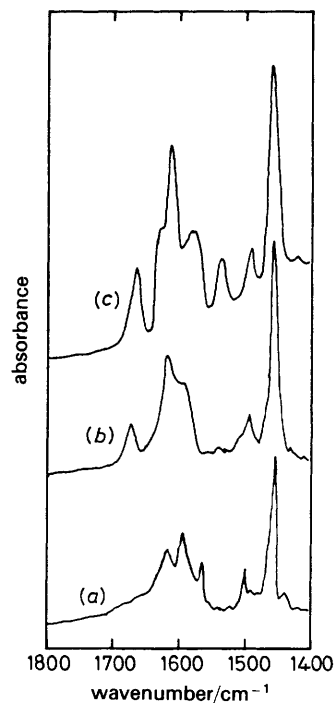
**Table 2** Textural properties of AIP catalysts: pore-size distribution for samples as prepared at 670 K

sample	< 15 Å	15–30 Å	> 30 Å
AIP0	98.4	1.6	0.0
AIP2	81.7	18.1	0.2
AIP5	96.6	3.2	0.2
AIP7	90.0	9.8	0.2
AIP10	95.7	3.9	0.4
AIP12	95.0	4.4	0.6
AIP15	85.1	13.4	1.5

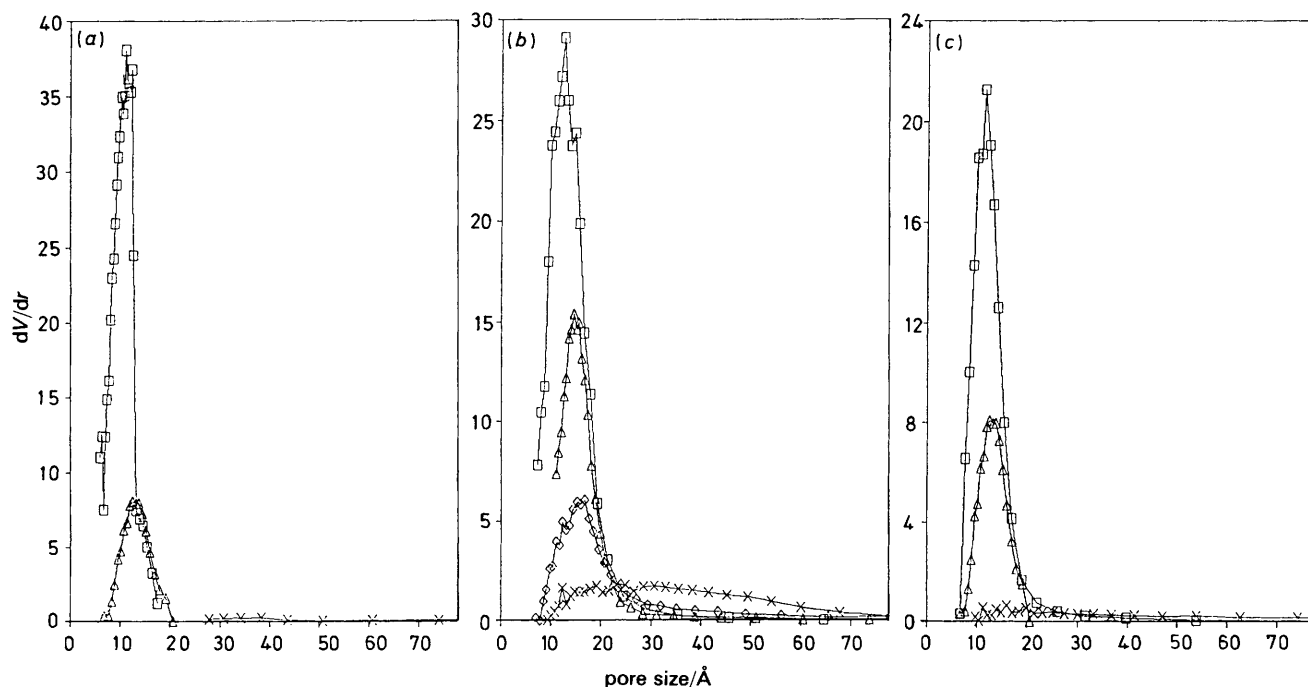
maximum (shifted to near 15 Å at most) (Table 2), but causes a proportional decrease in the shape of the distribution curve as evidenced in Fig. 7, according to the decrease of the surface area. By increasing the temperature of final treatment a broadening of the curves and a shift of the peak at higher values of radius is observed on all samples, according to a progressive coalescence of pores parallel to the drop in the surface area. In any case all amorphous samples show a monomodal pore distribution with the maximum below 20 Å.

#### FTIR Study of Pyridine Adsorption

As previously done for both  $\alpha\text{-Al}_2\text{O}_3$ <sup>19</sup> and transition aluminas<sup>20,21</sup> we have attempted an FTIR spectroscopic

**Fig. 8** FTIR spectra of pyridine adsorbed on AIP0 (a), AIP2 (b) and AIP10 (c) at 20 °C, after evacuation at 20 °C

characterization of the surface acidity of these materials using pyridine as a probe molecule. In Fig. 8 the spectra of pyridine adsorbed at room temperature on AIP0, AIP2 and AIP10 are compared. The spectrum of pyridine adsorbed on AIP0 has been discussed elsewhere.<sup>4</sup> The two bands observed near 1615 and 1595  $\text{cm}^{-1}$  are relative to the most sensitive  $\nu_{8a}$  mode of two different adsorbed species. The lower-frequency mode is due to pyridine interacting with weak Lewis sites (sites III) identified by Morterra *et al.*<sup>20,21</sup> as coordinatively unsaturated nearly octahedral  $\text{Al}^{3+}$  ions. The band at 1615  $\text{cm}^{-1}$  is due to pyridine species coordinated on Lewis sites of medium acidity, involving (following again Morterra *et*

**Fig. 7** Pore-size distributions of AIP0 (a), AIP2 (b) and AIP7 (c) after treatment at 670 K (□), 1070 K (Δ), 1230 K (◇) and 1370 K (×)

*al.*<sup>19,20</sup>) both octahedral and tetrahedral sites. All other bands are due to pyridine species interacting with Lewis sites. No Brønsted acids able to protonate pyridine are consequently present on the surface of amorphous alumina as on its crystalline forms.<sup>19–21</sup> On AIP2 almost the same spectrum is observed with the presence of a more weak absorption near 1650  $\text{cm}^{-1}$  which is very likely to be due to pyridinium cations. Their presence is very probably associated with the presence of surface phosphate species that, in the absence of very strong evacuation pretreatments, are in the form of Brønsted-acidic hydrogen phosphate ions. This compares with the behaviour reported for alumina impregnated by phosphoric acid,<sup>15</sup> and for  $\text{AlPO}_4$ .<sup>9,10</sup>

Several features absent in the spectrum of the species adsorbed on AIP0 are observed for that adsorbed on AIP10. In particular, the small bands at 1660 and 1535  $\text{cm}^{-1}$  may be assigned to pyridinium cations, produced by reaction of pyridine with surface Brønsted sites. It is, however, remarkable that these bands are very weak, suggesting (according to the relative absorption coefficients of the bands of the two species) that these sites are very few, in respect to the sites responsible for molecular pyridine adsorption. Moreover, together with the two  $\nu_8a$  vibrational bands observed on AIP0, a shoulder near 1625  $\text{cm}^{-1}$  is also observed in the case of AIP10. According to the increase in this frequency this shoulder is due to pyridine interacting with stronger Lewis sites, called type I sites, identified as very strongly acidic coordinatively unsaturated tetrahedral  $\text{Al}^{3+}$  exposed ions.<sup>19,20</sup> As discussed previously, these sites, present on transition aluminas such as  $\gamma$ -,  $\delta$ - and  $\eta$ -aluminas,<sup>20,21</sup> are absent or are very few on amorphous alumina<sup>4</sup> as on the  $\alpha$  phase.<sup>19</sup> The presence of phosphate species would then induce the presence of these sites even on amorphous alumina. We remark that neither Peri<sup>9</sup> nor Tada<sup>10</sup> in their studies of pyridine adsorbed on  $\text{AlPO}_4$  observed this band. The presence of Al cations in tetrahedral environments when phosphate species are present is reasonable taking into account that all crystalline forms of  $\text{AlPO}_4$  have this coordination state for  $\text{Al}^{3+}$ .

### Catalytic Activity in Methanol Conversion

The catalytic activity in methanol conversion has been investigated at temperatures where the samples are still in the amorphous state. Fig. 9 shows that the real rate of reaction observed followed the order (AIP0 < AIP2 < AIP5 < AIP7 < AIP10) > AIP12  $\approx$  AIP15. In all cases the reaction rate increases with the temperature but at the higher temperatures the observed rates are influenced by the reaction equilibrium. Thus at the higher temperatures the observed differences of

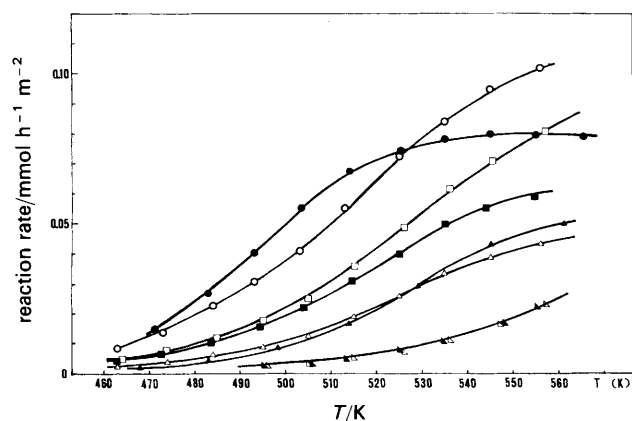


Fig. 9 Effect of the reaction temperature on the rate of methanol dehydration on AIP catalysts; ▲, AIP0; △, AIP2; ■, AIP5; □, AIP7; ○, AIP10; ▽, AIP12; ▲, AIP15; ●, commercial  $\gamma$ - $\text{Al}_2\text{O}_3$

catalytic activity can be essentially ascribed to the different surface area of the samples.

A suitable evaluation of the relative catalytic activity can be obtained at a low level of conversion (*ca.* 10%) in the range 470–490 K. In Table 1 the reaction rates at 495 K are reported. The experimental data show that the increase of activity was related to the amount of phosphorus contained in the catalyst up to a 10% content (AIP10). Above this value the catalytic activity collapses.

The low activity of the amorphous pure alumina evidences the role of phosphorus as activator in the mechanism involved in the methanol dehydration. The fact that the reaction rate of the most active sample (AIP10) is very close to the activity of a commercial  $\gamma$ -alumina can suggest that the surface sites on the two catalysts are similar as far as the type and concentration are concerned.

### Conclusions

Following the above experimental data we may conclude that high-surface microporous amorphous  $\text{Al}_2\text{O}_3$ - $\text{AlPO}_4$  mixed catalysts may be prepared by the reductive decomposition of Al nitrate with phosphoric acid. These materials retain an amorphous character and show a 'zeolite'-type microporosity even after calcination at temperatures of the order of 1370 K. The presence of phosphate ions in small amounts (up to 15 atom %) hinders the crystallization of the  $\gamma$ - $\text{Al}_2\text{O}_3$  phase, so favouring the stability of the amorphous state. The microstructure of these materials is comparable to those of amorphous alumina prepared by different methods described recently by Teichner and co-workers,<sup>2</sup> although the surface area and the stability of the amorphous phase are even higher.

IR studies of pyridine adsorption and catalytic activity in methanol dehydration indicate that these materials at low P content display a weak Lewis acidity and, if P is present, also Brønsted acidity. The weak Lewis acidity is probably related to the predominance of octahedrally coordinated  $\text{Al}^{3+}$  ions, as already found on amorphous aluminas<sup>4,5</sup> and also on  $\text{Al}_2\text{O}_3$ - $\text{P}_2\text{O}_5$  glasses.<sup>14</sup> Brønsted acidity is instead generated by surface hydrogenphosphate ions, as already found for  $\gamma$ -alumina impregnated by phosphoric acid<sup>15</sup> and on  $\text{AlPO}_4$ .<sup>9,10</sup>

The increase of P-content up to 10 atom % apparently favours the formation of tetrahedrally coordinated  $\text{Al}^{3+}$  ions, possibly because of the formation of  $\text{AlPO}_4$  microdomains. This compound in fact contains, in all its many crystal phases, tetrahedrally coordinated Al. The progressive formation of these sites, which when exposed on the surface can be coordinatively unsaturated and generate strong Lewis acidity similar to that of  $\text{AlPO}_4$ <sup>9,10</sup> and of transitional aluminas,<sup>20,21</sup> can explain the enhancement of the catalytic activity in methanol dehydration to dimethyl ether of the samples when the P content rises from 0 to 10 atom %. In fact, dissociative adsorption of methanol on alumina is thought to take place just on these strong Lewis sites,<sup>22</sup> producing methoxy species that would act as intermediates by reaction with gas phase methanol giving dimethyl ether. According to the detection of these strong Lewis sites catalytic activity of the AIP10 sample resembles that of a commercial  $\gamma$ - $\text{Al}_2\text{O}_3$  sample. The interpretation of the drop in the catalytic activity of the samples containing more than 10% atoms is more difficult. However, it is possible that  $\text{P}_2\text{O}_5$  or  $\text{H}_3\text{PO}_4$  when present in sufficient amounts tend to segregate on the surface of the amorphous material calcined at a temperature as low as 670 K, so covering the Lewis sites.

The studies of the thermal stability of these materials indicate that the presence of phosphate ions increasingly inhibits

the crystallization of the  $\gamma$ -alumina phase. This is reasonable, considering that  $\text{AlPO}_4$  simultaneously crystallizes in these samples. The crystallization of these materials implies a phase separation, that can be more difficult if the P amount is high. Also the  $\gamma$ -to- $\alpha$  alumina transition is inhibited by phosphate species. However, this effect is only shown by comparing the behaviour of pure alumina AlP0 with that containing 2% P (AlP2). This can be reasonably explained supposing a small solubility of  $\text{AlPO}_4$  in  $\gamma\text{-Al}_2\text{O}_3$ , whose presence would hinder the transformation to the  $\alpha$ -phase. However, it has been shown that even by impregnating  $\gamma$ -alumina with phosphoric acid, the  $\gamma$ -to- $\alpha$  transition is inhibited. We can propose, consequently, that phosphoric acid tends to lie on the surface of  $\gamma$ -alumina and to inhibit its transformation due to a surface effect. Similar surface effects have been reported in the case of the anatase-to-rutile  $\text{TiO}_2$  phase transformation.<sup>23,24</sup>

This research was funded by MPI (Ministero Pubblica Istruzione-Fondi 40%).

## References

- 1 D. L. Cocke, E. D. Johnson and R. P. Merrill, *Catal. Rev. Sci. Eng.*, 1984, **26**, 163.
- 2 G. Tournier, M. Lacroix-Repellin, G. M. Pajonk and S. J. Teichner, in *Preparation of Catalysts IV*, ed. B. Delmon, P. Grange, P. A. Jacobs and G. Poncelet (Elsevier, Amsterdam 1987), p. 333.
- 3 A. J. Fanelli, J. W. Burlew and G. B. Marsh, *J. Catal.* 1989, **116**, 318.
- 4 F. Abbattista, S. Delmastro, G. Gozzelino, D. Mazza, M. Vallino, G. Busca, V. Lorenzelli and G. Ramis, *J. Catal.*, 1989, **117**, 42.
- 5 P. Nortier, P. Fourre, A. B. Mohammed Saad, O. Saur and J. C. Lavalley, submitted paper; personal communication.
- 6 J. M. Thomas and J. Klinowski, *Adv. Catal.*, 1985, **33**, 199.
- 7 K. P. Peil, L. G. Galya and G. Marcelin, *J. Catal.*, 1989, **115**, 441.
- 8 J. B. Moffat, *Catal. Rev. Sci. Eng.*, 1978, **18**, 199.
- 9 J. B. Peri, *Discuss. Faraday Soc.*, 1971, **52**, 55.
- 10 A. Tada, *Mater. Chem. Phys.*, 1987, **17**, 145.
- 11 A. Schmidmeyer and J. B. Moffat, *Mater. Chem. Phys.*, 1985, **13**, 409.
- 12 J. M. Campelo, A. Garcia, D. Luna, J. M. Marinas and M. I. Martinez, *Mater. Chem. Phys.*, 1989, **21**, 409.
- 13 T. Kanazawa, *Inorganic Phosphate Materials* (Elsevier, Amsterdam 1989).
- 14 D. Muller, G. Berger, I. Grunze, G. Ladwig, E. Hallas and U. Haubenreisser, *Phys. Chem. Glasses*, 1983, **24**, 37.
- 15 G. Ramis, P. F. Rossi, G. Busca, V. Lorenzelli, A. La Ginestra and P. Patrono, *Langmuir*, 1989, **5**, 917.
- 16 K. Gishti, A. Iannibello, S. Marengo, G. Morelli and P. Tittarelli, *Appl. Catal.*, 1984, **12**, 381.
- 17 G. D. Hasley, *J. Chem. Phys.*, 1948, **16**, 931.
- 18 M. I. Baraton and P. Quintard, *J. Mol. Struct.*, 1982, **79**, 337.
- 19 C. Morterra, S. Coluccia, A. Chiorino and F. Boccuzzi, *J. Catal.*, 1978, **54**, 348.
- 20 A. Morterra, A. Chiorino, G. Ghiotti and E. Garrone, *J. Chem. Soc., Faraday Trans. 1*, 1979, **75**, 271.
- 21 H. Knozinger and P. Ratnasami, *Catal. Rev. Sci. Eng.*, 1978, **17**, 31.
- 22 G. Busca, P. F. Rossi, V. Lorenzelli, M. Benaissa, J. Travert and J. C. Lavalley, *J. Phys. Chem.*, 1985, **89**, 5433.
- 23 G. Oliveri, G. Busca and V. Lorenzelli, *Mater. Chem. Phys.*, 1989, **22**, 511.
- 24 J. Criado and C. Real, *J. Chem. Soc., Faraday Trans. 1*, 1983, **79**, 2765.

Paper 0/00995D; Received 6th March, 1990